RSC Advances

PAPER

View Article Online
View Journal | View Issue

Cite this: *RSC Adv.*, 2016, **6**, 13964

Influence of the non-conjugated 5-position substituent of 1,3,5-triaryl-2-pyrazoline-based photosensitizers on the photophysical properties and performance of a dye-sensitized solar cell†

Takeshi Mori,*[a] Hitoshi Saomoto,[a] Koji Machitani,[a] Kaname Inoue,[b] Yasunori Aoki,[b] Takeshi Koshitani,[b] Nagatoshi Koumura[c] and Takurou N. Murakami*[c]

Received 10th January 2016
Accepted 22nd January 2016

DOI: 10.1039/c6ra00738d

www.rsc.org/advances

We report the effect of the non-conjugated 5-position substituent of pyrazoline-based photosensitizers on the photophysical characteristics and performance of dye-sensitized solar cells (DSSCs). Four photosensitizers which contained different *para*-substituted phenyl groups (dimethylamine (**6a**), hexyloxy (**6b**), ethyl ester (**6c**), and no substituent (**6d**)) at the 5-position were synthesized. Although these substituents were not part of the conjugated π-system of the pyrazoline, their absorption maxima showed a red shift from 496 to 510 nm with increasing electron-donating ability. The same trend was observed for their electrochemical characteristics: the oxidation potentials decreased from 1.14 to 0.97 V. In terms of DSSC performance, **6a**, which had a strongly electron donating substituent at the 5-position, delivered the highest short-circuit current (J_{sc}) of 12.3 mA cm^{-2}, an incident photon-to-current conversion efficiency (IPCE) as high as 75%, and the best power conversion efficiency (PCE, η) of 5.7% under AM 1.5 G conditions. Further investigation with the stepped light-induced photocurrent and voltage transients (SLIM-PCV) method revealed that the steric differences between the groups at the 5-position clearly influenced the recombination reaction, resulting in the highest V_{oc} of 636 mV in the DSSC employing **6a** with the bulky dimethylamine substituent.

1. Introduction

Over the past few decades, photosensitizers in dye-sensitized solar cells (DSSCs) have been extensively investigated in order to expand their use as flexible, portable, and colorful photoenergy-conversion applications.[1,2] Although worldwide interest in the development of perovskite-based solar cells has grown recently,[3,4] DSSCs still attract much attention in the light-harvesting device market for use under room lighting. Among DSSCs, photosensitizers based on ruthenium complexes have achieved the best power conversion efficiencies (PCE, η), exceeding 11% as measured by the standard method (with over 1 cm^2 illumination area), which are comparable to the PCE values of amorphous silicon solar cells.[5,6] However, in terms of practical applications, ruthenium is a scarce resource and can be expensive. Owing to these limitations, considerable effort has gone into developing ruthenium-free photosensitizers. The key strategy for synthesizing ruthenium-free photosensitizers with high PCEs is the design of donor–π–acceptor structures which enable the efficient transfer of electrons from an electron-donating group to an electron-withdrawing group anchored to the surface of TiO_2.[7] In addition, strong intramolecular charge transfer allows for the realization of light absorption over a wide range, spanning the entire visible region. Based on this ideal model, a number of D–π–A photosensitizers have been prepared, including coumarins,[8] cyanines,[9–11] carbazoles,[12–16] triphenylamines,[17] and indolines[18] as donors. The resulting DSSCs with organic photosensitizers have exhibited PCE values of over 10%,[19,20] approaching those of the ruthenium-based photosensitizers.

Pyrazoline compounds have been widely investigated in bioorganic chemistry,[21–26] and utilized as optical brighteners, chemical sensors, and organic electronic materials.[27–34] Surprisingly, in spite of these attractive optical and electronic characteristics, pyrazolines have never been prepared as photosensitizers for DSSCs.

[a]*Industrial Technology Center of Wakayama Prefecture, Japan. E-mail: tmori@wakayama-kg.jp*

[b]*Nippon Chemical Works Co., Ltd., Japan*

[c]*Research Center for Photovoltaics, National Institute of Advanced Industrial Science and Technology (AIST), Japan. E-mail: takurou-murakami@aist.go.jp*

† Electronic supplementary information (ESI) available: Synthesis and characterization details; absorption spectra; photovoltaic performance details. See DOI: 10.1039/c6ra00738d

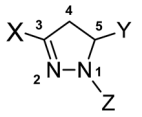

Chart 1 Pyrazoline ring positions.

One of specific advantages of pyrazolines is that various substituents can be introduced into the 1-, 3-, and 5-positions of the five-membered ring during synthesis (Chart 1). Thus, in the design of D–π–A structures incorporating pyrazolines for DSSCs, selecting the appropriate sites for the donor and acceptor units from among the three positions is the initial step. Preliminarily, we performed density functional theory (DFT) calculations for simple pyrazoline photosensitizers employing cyanoacrylic acid as the acceptor unit in each position. The results revealed that the donor and acceptor units should be located at the 1- and 3-positions, respectively, in order to accomplish effective electron transfer. Taking all of these considerations into account, we developed a series of pyrazoline photosensitizers. Specifically, in this paper, we report the effect of the substituent at the 5-position on the photophysical properties and DSSC performance using four novel photosensitizers (Fig. 1). The core structure of these photosensitizers consists of 4-(6-methylbenzothiazol-2-yl)phenyl as the donor unit, commonly used cyanoacrylic acid as the acceptor unit, and bithiophene as the π-bridge. Among the series of donor units we developed, 4-(6-methylbenzothiazol-2-yl)phenyl satisfied our requirement for low-cost mass production. The precursor of the donor unit, 4-(6-methylbenzothiazol-2-yl)phenyl hydrazine, is easily synthesized starting from toluidine, followed by dehydrothio-*p*-toluidine, which has been widely utilized as a key intermediate and chromophore for dyes and pigments. At the 5-position, *para*-substituted phenyl groups with different electronic characters (dimethylamino (NMe_2), hexyloxy (OC_6H_{13}), and ethyl ester (COOEt)) and the unsubstituted compound (H) were used. To elucidate the effect of the 5-position substituent, photophysical and electrochemical characterization and photovoltaic performance were investigated. Furthermore, to evaluate the recombination reaction, we investigated the electron lifetimes of the DSSCs.[35–37]

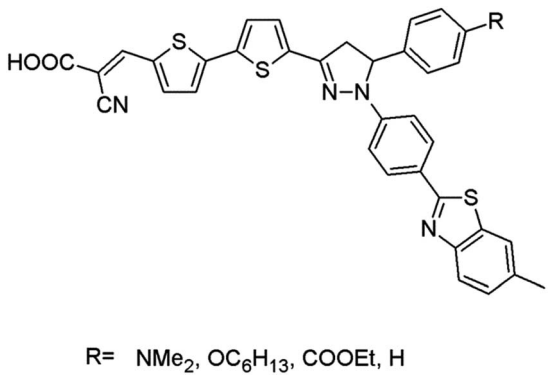

Fig. 1 Molecular structures of pyrazoline photosensitizers.

2. Experimental section

Photosensitizer characterization

^1H and ^{13}C NMR spectra were recorded on a Bruker Avance 400 MHz system. Chemical shifts are expressed in ppm using $CDCl_3$, DMSO-d_6, and acetone-d_6 as an internal standard. UV/vis measurements were performed with a Shimadzu UV-3101PC spectrometer in dilute solution. Oxidation potentials were obtained by differential pulse voltammetry with a BioLogic SP-300 system using a three-electrode cell consisting of a Pt-deposited fluorine-doped tin oxide (FTO) glass counter electrode, a dye-sensitized TiO_2 film on an FTO glass working electrode, and a $Ag/AgNO_3$ reference electrode. The potentials were calibrated against the ferrocene/ferrocenium (Fc/Fc^+) redox couple. Elemental analyses were performed with a Thermo Fisher Scientific FLASH 2000 CHNS/O analyzer. High-resolution mass spectrometry (HRMS) data were obtained with a Thermo Fisher Scientific Exactive™ system.

DSSC fabrication

The photoanodes were prepared by screen-printing a transparent layer of 20 nm TiO_2 particles (4 μm thick, 18NR-T, Dyesol) onto FTO conducting glass (Nippon Sheet Glass) pre-treated with 0.04 M aq. $TiCl_4$. The screen printed TiO_2 layer was sintered at 500 °C for 30 min. For an optimized TiO_2 layer, a scattering layer of 400 nm TiO_2 particles (3 μm thick, PST-400C, Catalysts & Chemicals Industries Co., Ltd.) was coated on the transparent layer, and after sintering, the double TiO_2 layer was treated with 0.01 M aq. $TiCl_4$ as a post-treatment. Before immersion in the dye bath (concentration: 0.3 mM in toluene) at 30 °C for 18 h, the photoanodes were sintered again at 450 °C for 30 min. The counter electrodes, comprising FTO conducting glass into which two holes had been drilled, were platinized by the heat deposition of hexachloroplatinic acid. Cell fabrication was carried out by thermally sealing the layers together with 35 μm-thick Surlyn®. The electrolyte was injected into the cell from the holes in the counter electrodes, and the holes were sealed with Surlyn® and a cover glass. All photovoltaic characteristics were measured using an electrolyte consisting of 0.6 M 1,3-dimethylimidazolium iodide, 0.05 M iodin 0.5 M *tert*-butylpyridine, and 0.1 M lithium iodide in acetonitrile (MeCN).

Measurements

The photocurrent–voltage characteristics were measured using a WACOM WXS-80C-3 solar simulator equipped with an AM 1.5 G filter and an ADVANTEST R6243 source/monitor. The light intensity (100 mW cm^{-2}) was calibrated using a reference silicon photovoltaic cell. A metal mask with an aperture area of 0.16 cm^2 was used to normalize the active area. The incident photon-to-current conversion efficiency (IPCE) spectra were measured with a Bunko Keiki CEP-99W system. The stepped light-induced photocurrent and voltage transients (SLIM-PCV) method was used to obtain the electron lifetimes, and the charge extraction technique was performed to evaluate the charge densities.[38] To calculate the charge density, the TiO_2 film thickness was exactly measured with a KLA Tencor Alpha-Step

500 system. The dye loading on TiO_2 was determined by the amount of desorbed dye from the dye-sensitized TiO_2 electrodes with tetrabutylammonium hydroxide (TBAOH, 10% aq.)/THF solution.

3. Results and discussion

Synthesis

The synthetic route for the pyrazoline photosensitizers is shown in Scheme 1. As previously reported, the pyrazoline core was easily synthesized *via* two condensations.[39–41] Initially, multi-functionalized chalcones **3a–d** were prepared through the Claisen–Schmidt condensation in the presence of NaOH at ambient temperature. In the case of compound **3c**, the direct condensation of **1** and ethyl-4-formylbenzoate produced a mixture containing a deprotected compound owing to hydrolysis under the basic conditions. Therefore, a carboxyl-substituted chalcone was prepared first; subsequent esterification with bromoethane successfully afforded **3c**. Condensation of chalcones **3a–d** with 4-(6-methylbenzothiazol-2-yl)phenylhydrazine under acidic conditions yielded the pyrazoline cores **4a–d**. To extend the π-bridge of the pyrazolines, another thiophene unit was introduced by a Suzuki–Miyaura coupling reaction, leading to the aldehyde-functionalized D–π units **5a–d**. Finally, the introduction of the acceptor unit by the Knoevenagel reaction of the aldehydes with 2-cyanoacetic acid in the presence of piperidine gave novel photosensitizers **6a–d**. All new compounds were confirmed by NMR, elemental analysis, and HRMS (see ESI for details†).

Photophysical and electrochemical properties of the photosensitizers

The absorption spectra of the photosensitizers were measured as solutions in tetrahydrofuran (THF) and as adsorbed on a TiO_2 film. Fig. 2 shows the solution absorption spectra and Table 1 summarizes the photophysical data. The photosensitizers in solution show similar absorption spectra in the visible light region, with two bands at approximately 390 and 510 nm tailing up to 610 nm. For all the photosensitizers, higher-energy bands corresponding to π–π* transitions are observed in almost the same region at 390 nm. For the lower energy bands, corresponding to intramolecular charge transfer (ICT) transitions, the absorption maxima are red-shifted in the order **6a** (510 nm) > **6b** (505 nm) > **6d** (502 nm) > **6c** (496 nm). Interestingly, this order is related to the electron-donating ability of the 5-position phenyl substituent, $NMe_2 > OC_6H_{13} > H >$ COOEt, even though it does not contribute directly to the conjugated π–system along the 1- through 3-positions. This tendency was also found in the optical band-gap (E_g) widening, which occurred in the order **6a** (2.04 eV) < **6b** (2.05 eV) < **6c** and **6d** (2.06 eV), indicating the weakening of the electron-donating ability. These values were estimated from the onset of the absorption spectra of a sensitized thin TiO_2 film (see ESI†). This might suggest that the electronic nature of the substituent at the 5-position of the pyrazoline ring has an influence on the ICT interaction between the donor at the 1-position and the acceptor at the 3-position.

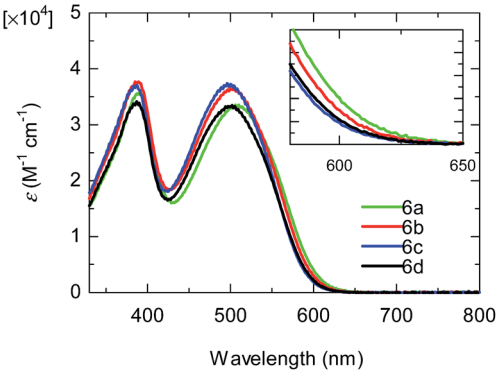

Fig. 2 Absorption spectra of **6a–d** in THF. The inset shows the absorption onsets.

To further investigate the effect of the 5-position substituent, differential pulse voltammetry (DPV) was performed to understand the differences in the oxidation potentials, *i.e.*, the highest occupied molecular orbital (HOMO) levels, of the photosensitizers. All potentials were obtained against a Ag/$AgNO_3$ reference electrode in 0.1 M tetrabutylammonium perchlorate ($TBAClO_4$) in MeCN, and calibrated with the Fc/Fc^+ redox couple (0.62 V *versus* NHE).[42,43] To observe the electrochemical behaviors under the same conditions as in the DSSCs,

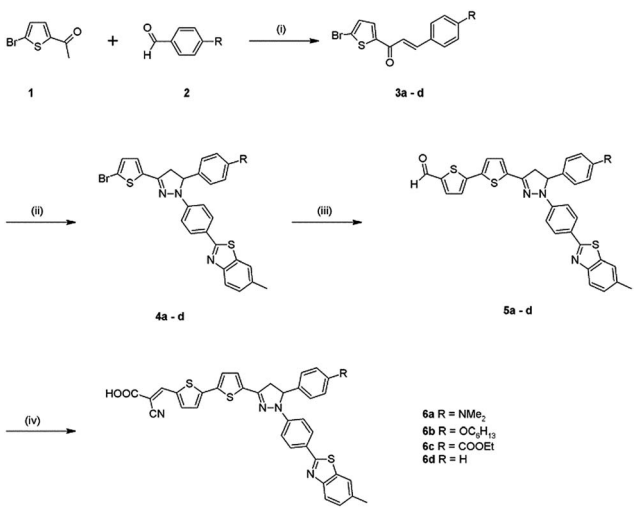

Scheme 1 Synthetic route for pyrazoline-based photosensitizers **6a–d**.

Table 1 Photophysical properties and estimated dye loading of **6a–d**

	UV-vis			
Dye	λ_{max} in THF (nm)	ε (M^{-1} cm^{-1})	λ_{max} on TiO_2 (nm)	Dye loading (10^{-4} mol cm^{-3})
6a	510	33 591	465	2.8
6b	505	36 511	465	2.9
6c	496	37 390	456	2.4
6d	502	33 511	458	2.4

Table 2 Electrochemical properties of **6a–d** measured by differential pulse voltammetry[a]

Dye	E_{ox} *vs.* NHE[b] (V)	E_g[c] (eV)	E_{red} *vs.* NHE[d] (V)	HOMO[e] (eV)	LUMO[f] (eV)
6a	0.97	2.04	−1.07	−5.15	−3.11
6b	1.09	2.05	−0.96	−5.27	−3.22
6c	1.14	2.06	−0.92	−5.32	−3.26
6d	1.10	2.06	−0.96	−5.28	−3.22

[a] Measured in 0.1 M $TBAClO_4$ in MeCN. [b] Calibrated with Fc/Fc^+ (0.62 V *vs.* NHE). [c] Estimated from the onset of absorption spectrum on TiO_2. [d] Calculated using $E_{red} = E_{ox} - E_g$. [e] Calibrated with the HOMO of $Fc/Fc^+ = -4.8$ eV. [f] Estimated from HOMO + E_g.

Table 3 Photovoltaic parameters of **6a–d** measured under AM 1.5 G (100 mW cm^{-2})

Dye	J_{sc} (mA cm^{-2})	V_{oc} (mV)	FF	η (%)
6a	10.3	654	0.74	5.0
6b	9.65	640	0.73	4.5
6c	8.85	625	0.73	4.0
6d	9.09	621	0.73	4.1

a dye-sensitized TiO_2 film on FTO glass was used as the working electrode. The oxidation potentials (E_{ox}) are listed in Table 2. The order of the oxidation potentials from low to high was **6a**, **6b**, **6d**, and **6c**. This result indicates that the HOMO levels are influenced by the electronic nature of the 5-position substituent; thus, the electron-donating NMe_2 unit in **6a** affords 0.17 V lower oxidation energy than that of **6c**.

The HOMO levels of all the photosensitizers are satisfactorily more positive than the redox potential of I^-/I_3^- (0.37 V *versus* NHE), to regenerate the oxidized photosensitizers.[44] The reduction potentials (E_{red}) corresponding to the lowest unoccupied molecular orbital (LUMO) must be more negative than the conduction band edge level of TiO_2 (−0.5 V *versus* NHE) to ensure sufficient charge injection.[8] The LUMO levels, estimated from the equation $E_{ox} - E_g$, were low enough for charge injection to TiO_2 for all the photosensitizers. Among them, **6a** possessed the greatest charge injection driving force of 0.57 V and a longer absorption-onset wavelength, leading to an increased photocurrent.

Photovoltaic performance

The photovoltaic performance of the DSSCs with the four photosensitizers was measured under AM 1.5 G (100 mW cm^{-2}). To elucidate the performance differences among the photosensitizers, a 4 μm-thick transparent single-layer TiO_2 film was used for the photoanode without $TiCl_4$ post-treatment to eliminate other effects, except for the electronic and structural effects from the photosensitizers themselves.

The current density (J)–voltage (V) curves are shown in Fig. 3, and the typical photovoltaic parameters are listed in Table 3. All data were obtained with high reproducibility, and the average data are shown in Table S1 (ESI†). The short-circuit currents (J_{sc}) are consistent with the electron-donating ability of the 5-position substituent. The highest value (10.3 mA cm^{-2}) was obtained in the cell employing **6a**, whereas that of **6c** was the lowest (8.85 mA cm^{-2}). The IPCE spectra are shown in Fig. 4. The highest IPCE values from 400 to 600 nm of **6a** and **6b** are comparable, and the highest among the present photosensitizers. These results indicate that the highest J_{sc} of **6a** is due to the absorption onset found in the longest wavelength of all the photosensitizers. In the case of **6c**, the lower IPCE value at around 450 nm than that of **6b** and slightly narrower spectrum than **6d** decreases its photocurrent, resulting in the lowest J_{sc}. On the other hand, since there is no correlation between the highest value of the IPCE and the molar extinction coefficient, the electron injection efficiency or the reduction efficiency of the oxidized photosensitizers might influence the IPCE values. The open-circuit voltage (V_{oc}) values are 654, 640, 625, and 621 mV for **6a**, **6b**, **6c**, and **6d**, respectively; also, the onset voltages of the dark currents are ordered **6a** > **6b** > **6c** > **6d**. These results clearly indicate that there is no correlation with the electron-donating ability of the 5-position substituent. To explain the difference in the V_{oc} values among the photosensitizers, we investigated the charge recombination process.

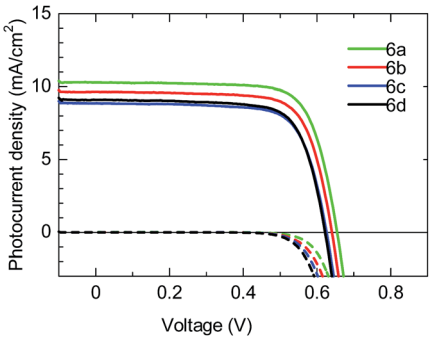

Fig. 3 J–V curves of DSSCs with a single-layer TiO_2 film employing **6a–d** under illumination (solid line) and in the dark (dashed line).

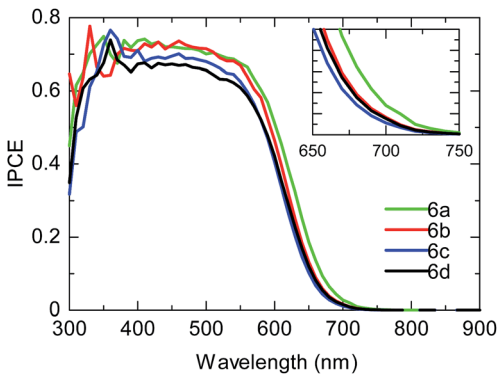

Fig. 4 IPCE of DSSCs with single-layer TiO_2 films employing **6a–d**. The inset shows the IPCE onsets.

Charge recombination

The SLIM-PCV and charge extraction methods are powerful tools for obtaining information on the charge recombination reaction at the interface between TiO_2 and the electrolyte. It is well known that the charge recombination process is a crucial contributor to the V_{oc} value. The electron concentration in TiO_2 significantly decreases with the recombination reaction in the DSSC. Therefore, recombination leads to a positive shift of the Fermi level in TiO_2, resulting in a decrease of V_{oc} with decreasing offset potential between the electrolyte redox potential and the Fermi level. Thus, observing the charge recombination process is important for improving DSSC performance. Fig. 5 shows the electron lifetime and the open-circuit voltage *versus* electron density of the DSSCs. The same tested cells were used as for the measurement of photovoltaic performance. Fig. 5a presents the data for the relationship between V_{oc} and the electron density for all the photosensitizers. These results indicate that the conduction band edge level of TiO_2 is not changed by the adsorbed photosensitizers. In the relationship between the electron lifetime *versus* electron density, the electron lifetime increases in the order **6a** > **6b** > **6c** > **6d**. The longer electron lifetime of **6a** is probably derived from the steric effects of the dimethylamino group on the 5-position substituent. Compared to the linear substituent of **6b**, the sterically bulky substituent of **6a** prevents iodide ions from approaching the TiO_2 surface, leading to suppression of the charge recombination

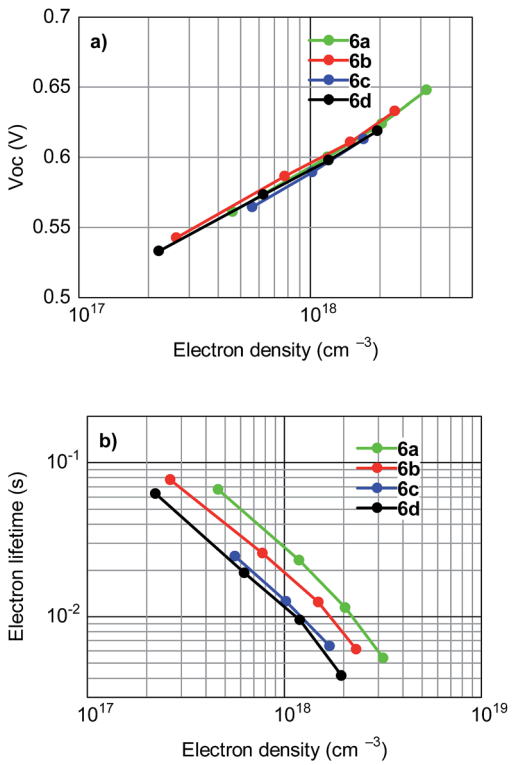

Fig. 5 (a) Plots of V_{oc} against electron density measured by the SLIM-PCV and charge extraction methods, and (b) plots of electron lifetime against electron density.

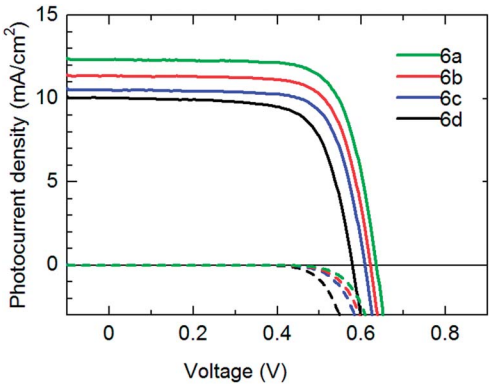

Fig. 6 *J–V* curves of DSSCs with a double-layer TiO_2 film employing **6a–d** under illumination (solid line) and in the dark (dashed line).

and the improvement of V_{oc} in the *J–V* curves.[45] In the cases of **6c** and **6d**, the less bulky or absent substituent on the phenyl ring cannot prevent charge recombination. In addition, the shorter electron lifetimes of **6c** and **6d** might be the cause of the slightly lower dye loading on TiO_2 than that of **6a**. As expected, the lower dye coverage of the TiO_2 surface for **6c** and **6d** unfavorably provides both electron-leakage and electrolyte-approaching paths, which enable a greater degree of charge recombination and result in the decreasing V_{oc}.

Finally, to investigate the best photovoltaic performance using the pyrazoline-based photosensitizers, DSSCs consisting of transparent and scattering TiO_2 photoanode layers were prepared. Fig. 6 shows their *J–V* curves, and the photovoltaic parameters are listed in Table S2.† With a broad absorption and a bulky substituent, the highest J_{sc} of 12.3 mA cm^{-2} and V_{oc} of 636 mV were obtained with **6a**, resulting in the best PCE of 5.7%.

4. Conclusion

In this work, we successfully synthesized new photosensitizers based on a 1,3,5-triaryl-2-pyrazoline core for DSSCs, and focused on investigating the effects of the 5-position substituent. We found that the electronic nature of the 5-position substituent had a significant influence on the photophysical and electrochemical characteristics of the DSSCs, even though it is not a part of the conjugated system of the pyrazoline. The absorption maxima and onset shifted toward longer wavelengths in the order NMe_2 (**6a**) > OC_6H_{13} (**6b**) > H (**6d**) > COOEt (**6c**). With the broader light absorption of **6a**, the DSSC with **6a** showed the highest J_{sc}. To increase the photocurrent, the electronic characteristics of the pyrazoline-based photosensitizers can be tuned by modifying the substituent at the 5-position without altering the entire conjugated system. We also found that the structural effects of the 5-position substituent are important to improving the V_{oc}. The electron lifetime measurements showed that the bulky substituent of **6a** suppresses the recombination reaction, resulting in the highest V_{oc} of 636 mV. The DSSC with

6a showed the highest PCE of 5.7% with a double-layer TiO_2 electrode.

Although the structures of the pyrazoline photosensitizers were not fully optimized for DSSCs in this work, promising performance improvements were obtained. With these results, we will continue our research to develop high-performance pyrazoline photosensitizers.

Acknowledgements

We thank H. Kodama for helpful assistance. Financial support from AIST and Wakayama prefecture is gratefully acknowledged.

Notes and references

1 B. O'Regan and M. Gratzel, *Nature*, 1991, **353**, 737–740.
2 A. Hagfeldt, G. Boschloo, L. Sun, L. Kloo and H. Pettersson, *Chem. Rev.*, 2010, **110**, 6595–6663.
3 A. Kojima, K. Teshima, Y. Shirai and T. Miyasaka, *J. Am. Chem. Soc.*, 2009, **131**, 6050–6051.
4 M. A. Green, A. Ho-Baillie and H. J. Snaith, *Nat. Photonics*, 2014, **8**, 506–514.
5 Y. Chiba, A. Islam, Y. Watanabe, R. Komiya, N. Koide and L. Han, *Jpn. J. Appl. Phys.*, 2006, **45**, L638.
6 F. Gao, Y. Wang, D. Shi, J. Zhang, M. Wang, X. Jing, R. Humphry-Baker, P. Wang, S. M. Zakeeruddin and M. Grätzel, *J. Am. Chem. Soc.*, 2008, **130**, 10720–10728.
7 A. Mishra, M. K. R. Fischer and P. Bäuerle, *Angew. Chem., Int. Ed.*, 2009, **48**, 2474–2499.
8 K. Hara, T. Sato, R. Katoh, A. Furube, Y. Ohga, A. Shinpo, S. Suga, K. Sayama, H. Sugihara and H. Arakawa, *J. Phys. Chem. B*, 2003, **107**, 597–606.
9 Z.-S. Wang, F.-Y. Li and C.-H. Huang, *Chem. Commun.*, 2000, 2063–2064.
10 E. Stathatos, P. Lianos, A. Laschewsky, O. Ouari and P. Van Cleuvenbergen, *Chem. Mater.*, 2001, **13**, 3888–3892.
11 Q.-H. Yao, L. Shan, F.-Y. Li, D.-D. Yin and C.-H. Huang, *New J. Chem.*, 2003, **27**, 1277–1283.
12 N. Koumura, Z.-S. Wang, S. Mori, M. Miyashita, E. Suzuki and K. Hara, *J. Am. Chem. Soc.*, 2008, **130**, 4202–4203.
13 Z.-S. Wang, N. Koumura, Y. Cui, M. Takahashi, H. Sekiguchi, A. Mori, T. Kubo, A. Furube and K. Hara, *Chem. Mater.*, 2008, **20**, 3993–4003.
14 T. N. Murakami, N. Koumura, M. Kimura and S. Mori, *Langmuir*, 2014, **30**, 2274–2279.
15 M. Paramasivam, R. K. Chitumalla, S. P. Singh, A. Islam, L. Han, V. Jayathirtha Rao and K. Bhanuprakash, *J. Phys. Chem. C*, 2015, **119**, 17053–17064.
16 S. S. Soni, K. B. Fadadu, J. V. Vaghasiya, B. G. Solanki, K. K. Sonigara, A. Singh, D. Das and P. K. Iyer, *J. Mater. Chem. A*, 2015, **3**, 21664–21671.
17 M. Liang and J. Chen, *Arylamine organic dyes for dye-sensitized solar cells*, 2013, vol. 42.
18 K. Pei, Y. Wu, H. Li, Z. Geng, H. Tian and W.-H. Zhu, *ACS Appl. Mater. Interfaces*, 2015, **7**, 5296–5304.
19 T. Horiuchi, H. Miura, K. Sumioka and S. Uchida, *J. Am. Chem. Soc.*, 2004, **126**, 12218–12219.
20 M. Matsui, M. Kotani, Y. Kubota, K. Funabiki, J. Jin, T. Yoshida, S. Higashijima and H. Miura, *Dyes Pigm.*, 2011, **91**, 145–152.
21 M. Amir, H. Kumar and S. a. Khan, *Bioorg. Med. Chem. Lett.*, 2008, **18**, 918–922.
22 E. Bansal, V. K. Srivastava and A. Kumar, *Eur. J. Med. Chem.*, 2001, **36**, 81–92.
23 I. G. Rathish, K. Javed, S. Ahmad, S. Bano, M. S. Alam, K. K. Pillai, S. Singh and V. Bagchi, *Bioorg. Med. Chem. Lett.*, 2009, **19**, 255–258.
24 K. L. Stirrett, J. a. Ferreras, V. Jayaprakash, B. N. Sinha, T. Ren and L. E. N. Quadri, *Bioorg. Med. Chem. Lett.*, 2008, **18**, 2662–2668.
25 O. I. El-Sabbagh, M. M. Baraka, S. M. Ibrahim, C. Pannecouque, G. Andrei, R. Snoeck, J. Balzarini and A. A. Rashad, *Eur. J. Med. Chem.*, 2009, **44**, 3746–3753.
26 P.-C. Lv, D.-D. Li, Q.-S. Li, X. Lu, Z.-P. Xiao and H.-L. Zhu, *Bioorg. Med. Chem. Lett.*, 2011, **21**, 5374–5377.
27 C. J. Fahrni, L. Yang and D. G. Vanderveer, *J. Am. Chem. Soc.*, 2003, **125**, 3799–3812.
28 J. F. Callan, a. P. De Silva and D. C. Magri, *Tetrahedron*, 2005, **61**, 8551–8588.
29 M. Verma, A. F. Chaudhry, M. T. Morgan and C. J. Fahrni, *Org. Biomol. Chem.*, 2010, **8**, 363–370.
30 P. M. Borsenberger and L. B. Schein, *J. Phys. Chem.*, 1994, **98**, 233–239.
31 X. H. Zhang, W. Y. Lai, Z. Q. Gao, T. C. Wong, C. S. Lee, H. L. Kwong, S. T. Lee and S. K. Wu, *Chem. Phys. Lett.*, 2000, **320**, 77–80.
32 M. Jin, Y. J. Liang, R. Lu, X. H. Chuai, Z. H. Yi, Y. Zhao and H. J. Zhang, *Synth. Met.*, 2004, **140**, 37–41.
33 T. Sano, Y. Nishio, Y. Hamada, H. Takahashi, T. Usuki and K. Shibata, *J. Mater. Chem.*, 2000, **10**, 157–161.
34 X. H. Zhang, S. K. Wu, Z. Q. Gao, C. S. Lee, S. T. Lee and H. L. Kwong, *Thin Solid Films*, 2000, **371**, 40–46.
35 S. Nakade, T. Kanzaki, Y. Wada and S. Yanagida, *Langmuir*, 2005, **21**, 10803–10807.
36 A. D. S. Gonçalves, M. R. Davolos, N. Masaki, S. Yanagida, S. Mori and A. F. Nogueira, *J. Appl. Phys.*, 2009, **106**, 064316.
37 M. Miyashita, K. Sunahara, T. Nishikawa, Y. Uemura, N. Koumura, K. Hara, A. Mori, T. Abe, E. Suzuki and S. Mori, *J. Am. Chem. Soc.*, 2008, **130**, 17874–17881.
38 N. W. Duffy, L. M. Peter, R. M. G. Rajapakse and K. G. U. Wijayantha, *Electrochem. Commun.*, 2000, **2**, 658–662.
39 M. J. Meyers, G. B. Arhancet, S. L. Hockerman, X. Chen, S. a. Long, M. W. Mahoney, J. R. Rico, D. J. Garland, J. R. Blinn, J. T. Collins, S. Yang, H. C. Huang, K. F. McGee, J. M. Wendling, J. D. Dietz, M. a. Payne, B. L. Homer, M. I. Heron, D. B. Reitz and X. Hu, *J. Med. Chem.*, 2010, **53**, 5979–6002.
40 G. Chen, H. Y. Wang, Y. Liu, X. P. Xu and S. J. Ji, *Dyes Pigm.*, 2010, **85**, 194–200.
41 H. Y. Wang, J. J. Shi, G. Chen, X. P. Xu and S. J. Ji, *Synth. Met.*, 2012, **162**, 241–246.

42 N. G. Connelly and W. E. Geiger, *Chem. Rev.*, 1996, **96**, 877–910.
43 C. M. Cardona, W. Li, A. E. Kaifer, D. Stockdale and G. C. Bazan, *Adv. Mater.*, 2011, **23**, 2367–2371.
44 J.-H. Yum, E. Baranoff, F. Kessler, T. Moehl, S. Ahmad, T. Bessho, A. Marchioro, E. Ghadiri, J.-E. Moser, C. Yi, M. K. Nazeeruddin and M. Grätzel, *Nat. Commun.*, 2012, **3**, 631.
45 N. Koumura, Z.-S. Wang, M. Miyashita, Y. Uemura, H. Sekiguchi, Y. Cui, A. Mori, S. Mori and K. Hara, *J. Mater. Chem.*, 2009, **19**, 4829–4836.